Robust Estimation of Dynamic and Algebraic States in Power Grids Using Penalized Weighted Least Squares and Cubature Kalman Filtering

Amir Dadashi, Amir Ameli
Electrical and Computer Engineering Department
Lakehead University
Thunder Bay, Ontario, Canada
adadashi@lakeheadu.ca, aameli@lakeheadu.ca

Hassan Naser
Software Engineering Department
Lakehead University
Thunder Bay, Ontario, Canada
hnaser@lakeheadu.ca

Mohsen Ghafouri
CIISE
Concordia University
Montreal, Quebec Canada
mohsen.ghafouri@concordia.ca

***Abstract*—The growing deployment of phasor measurement units (PMUs) and advanced communication technologies has elevated dynamic state estimation (DSE) as a critical tool for real-time monitoring and stability assessment. However, limited PMU coverage complicates the tracking of algebraic variables, and DSE performance remains vulnerable to false data injection attacks (FDIAs) and communication losses. This paper presents a hybrid approach that integrates penalized weighted least squares (PWLS) with a cubature Kalman filter (CKF) for DSE. By embedding nonlinear differential-algebraic equations into the CKF, the method jointly estimates dynamic and algebraic states, while PWLS enhances robustness by identifying and down-weighting compromised measurements. The proposed method is validated on the IEEE 39-bus test system under diverse attack scenarios.**

***Index Terms*—Dynamic state estimation, cubature Kalman filter, cyber-security, nonlinear differential-algebraic equations.**

I. Introduction

Modern power systems experience frequent operating-point changes due to renewable variability, stochastic generation, responsive loads, and distributed resources, violating the quasi-steady-state assumptions of traditional static state estimation. As a result, conventional monitoring tools are often inadequate. Dynamic state estimation (DSE), enabled by phasor measurement units (PMUs) and advanced communications, provides real-time tracking of system states, improving monitoring, stability assessment, and wide-area control and protection [1], [2].

Several Kalman filter (KF)–based methods, including Extended KF (EKF), Unscented KF (UKF), Ensembled KF [3], and Cubature KF (CKF) [4], have been applied to DSE to estimate the dynamic state variables of synchronous generators. To further improve these frameworks, the algebraic equations of the network can also be incorporated, enabling simultaneous estimation of algebraic variables in addition to dynamic ones. This provides broader network observability when optimal PMU placement cannot capture all critical variables, such as voltage phasors, at every location [5]. Such DSE frameworks have been proposed in [6]–[8] for the simultaneous real-time estimation of both dynamic and algebraic state variables. However, the performance of DSE remains highly dependent on accurate and reliable measurements, making it susceptible to cyber threats such as false data injection attacks (FDIAs) [9]; additionally, communication disruptions—resulting in delays or data loss—can further deteriorate measurement quality and ultimately compromise the estimation process [4]. Various strategies have been proposed in the literature to improve DSE robustness under such adverse conditions. For instance, the method in [10] jointly estimates system states and the attack vector by using an unknown input observer for state estimation followed by attack identification. Other robust statistics–based methods (e.g., [11]–[13]) reduce the impact of abnormal measurements by down-weighting large-deviation data using a generalized maximum-likelihood Kalman filter (GM-KF). Reference [14] improves estimation accuracy by embedding equality and inequality constraints into the DSE framework. Additionally, authors in [4] propose a resilient CKF-based DSE using the Cauchy kernel maximum correntropy criterion, which unifies state and measurement errors via statistical linearization and fixed-point iteration.

Despite their effectiveness in enhancing accuracy and mitigating cyber-attacks, existing methods exhibit key limitations: (i) reliance on linearized state-space models for computational simplicity; (ii) absence of explicit mechanisms to identify compromised measurements; and (iii) incomplete integration of algebraic equations, restricting the estimation of essential algebraic variables. In another approach, the authors in [9] integrate a PWLS algorithm into the EKF to detect and mitigate FDIAs by adaptively optimizing and downweighting measurement weights. However, this method estimates only the dynamic state variables. To address these challenges, this paper presents an algorithmic and structural enhancement of CKF-based DSE. The CKF is reformulated using a NDAE–based state-space model, enabling the simultaneous estimation of dynamic and algebraic state variables. In addition, the PWLS mechanism [9] is integrated into the CKF algorithm, improving robustness against corrupted or missing measurements. The resulting PWLS–CKF framework enhances the detection and mitigation of FDIAs and data loss while preserving estimation accuracy.

979-8-3315-8138-1

II. The Proposed Robust DSE Framework

A. NDAE-Based State-Space Model of Power Grid

To estimate the state variables via DSE, the discrete state-space model of the power system is expressed by

$$\boldsymbol{x}_{d,k} = f(\boldsymbol{x}_{k-1}, \boldsymbol{u}_{k-1}) + \boldsymbol{\mu}_d, \tag{1a}$$
$$0 = g(\boldsymbol{x}_k) + \boldsymbol{\mu}_a, \tag{1b}$$
$$\boldsymbol{z}_k = h(\boldsymbol{x}_k) + \boldsymbol{v}, \tag{1c}$$

where k is the time step; $\boldsymbol{x}_d$ denotes the dynamic state vector; $\boldsymbol{u}$ is the input vector; $f(.)$, $g(.)$, and $h(.)$ are the discretized dynamic, algebraic, and measurement functions, respectively, with $f(.)$ obtained via 4th-order Runge-Kutta [15]. The dynamic behavior of each generator is described by ordinary differential equations of (1a), while the network power flow is represented using algebraic KCL equations of (1b). This study employs the standard two-axis, 4th-order transient model of synchronous generators for accurate state estimation [15]. Based on this model, the state vector $\boldsymbol{x}$ is defined as

$$\boldsymbol{x} = [\boldsymbol{\delta}^\top \ \boldsymbol{\omega}^\top \ \boldsymbol{E}_q'^\top \ \boldsymbol{E}_d'^\top \ \boldsymbol{V}_R'^\top \ \boldsymbol{V}_I'^\top]^\top. \tag{2}$$

Here, $\boldsymbol{V}_R'$ and $\boldsymbol{V}_I'$ contain the real and imaginary parts of the non-generator bus voltages (p.u.); $\boldsymbol{\delta}$ is the rotor angle (rad); $\boldsymbol{\omega}$ is the rotor speed (rad/s); $\boldsymbol{E}_q'$ and $\boldsymbol{E}_d'$ are the transient voltages at the q and d axes (p.u.).

The algebraic equations in (1b) are derived by expressing generator terminal voltages in terms of dynamic states and non-generator bus voltages using the synchronous generator transient equivalent circuit [15], and substituting these into the KCL equations for non-generator buses.

The process and measurement noises, $\boldsymbol{\mu} = [\boldsymbol{\mu}_d^\top \ \boldsymbol{\mu}_a^\top]^\top$ and $\boldsymbol{v}$, account for model uncertainties, communication errors, and sensor inaccuracies, which are independent with covariances $E[\boldsymbol{\mu}\boldsymbol{\mu}^\top] = \boldsymbol{Q}_{k-1}$, $E[\boldsymbol{v}\boldsymbol{v}^\top] = \boldsymbol{R}_k$ [3]. In this study, the measurement vector $\boldsymbol{z}_k$, which is collected by the PMUs in the set $\mathcal{P}$, includes the real and imaginary parts of bus voltages and branch currents, given by

$$\boldsymbol{z}_k = [\boldsymbol{V}_R^\top \ \boldsymbol{V}_I^\top \ \boldsymbol{I}_{bR}^\top \ \boldsymbol{I}_{bI}^\top]_{\mathcal{P}}^\top \tag{3}$$

B. The Proposed Robust PWLS-CKF Method

DSE depends on fast, time-synchronized measurements to monitor system behavior in real time. It determines both dynamic and algebraic states by solving (1) while mitigating noise present in PMU measurements [1]. In this paper, the CKF is chosen for its nonlinear, derivative-free nature, high numerical accuracy, ease of scalability to high-dimensional systems, simple tuning, and robust performance under noise and strong nonlinearities compared with other KF methods [4]. In the following, the two-stage implementation of the proposed robust DSE algorithm is presented:

1) State Prediction: At this stage, the state variables at time step k are predicted using (1a) and (1b), based on the previously estimated states $\hat{\boldsymbol{x}}_{k-1}$ and the corresponding input variables $\boldsymbol{u}_{k-1}$. First, a set of cubature points based on the spherical–radial cubature rule is generated by

$$\hat{\boldsymbol{X}}_{i,k-1} = \boldsymbol{S}_{k-1}\boldsymbol{\zeta}_i + \hat{\boldsymbol{x}}_{k-1}, \quad i = 1, 2, \ldots, 2n \tag{4}$$

where n is the number of state variables. The matrix $\boldsymbol{S}_{k-1}$ is obtained by the Cholesky decomposition of the state error covariance matrix from the previous time step (i.e., $\boldsymbol{P}_{xx,k-1}$). Moreover, $\boldsymbol{\zeta}_i$ is defined as

$$\boldsymbol{\zeta}_i = \begin{cases} \sqrt{n}\boldsymbol{e}_i, & i = 1, 2, \ldots, n \\ -\sqrt{n}\boldsymbol{e}_i, & i = n+1, n+2, \ldots, 2n \end{cases} \tag{5}$$

where $\boldsymbol{e}_i \in \mathbb{R}^{n\times n}$ represents the identity matrix. Next, each cubature point is propagated through (1a) and (1b), producing the corresponding sets of transformed dynamic and algebraic samples, respectively, given by

$$\boldsymbol{X}_{di,k}^{*-} = f(\hat{\boldsymbol{X}}_{i,k-1}, \boldsymbol{u}_{k-1}) \tag{6}$$
$$g(\boldsymbol{X}_{di,k}^{*-}, \boldsymbol{X}_{ai,k}^{*-}) = 0 \tag{7}$$

Finally, the complete transformed cubature point is formed as $\boldsymbol{X}_{i,k}^{*-} = [\boldsymbol{X}_{id,k}^{*-\top} \ \boldsymbol{X}_{ia,k}^{*-\top}]$. By using them, the predicted state variables vector $\hat{\boldsymbol{x}}_k^-$ and the predicted state error covariance matrix $\boldsymbol{P}_{xx,k}^-$ can be calculated by

$$\hat{\boldsymbol{x}}_k^- = \frac{1}{2n}\sum_{i=1}^{2n} \boldsymbol{X}_{i,k}^{*-} \tag{8}$$

$$\boldsymbol{P}_{xx,k}^- = \frac{1}{2n}\sum_{i=1}^{2n} \left[\boldsymbol{X}_{i,k}^{*-}(\boldsymbol{X}_{i,k}^{*-})^\top - \hat{\boldsymbol{x}}_k^-(\hat{\boldsymbol{x}}_k^-)^\top\right] + \boldsymbol{Q}_{k-1} \tag{9}$$

2) State Correction: After the prediction step, the CKF correction step updates the predicted states using new PMU measurements. First, based on the state prediction above, a set of equal-weight cubature points, $\boldsymbol{X}_{i,k}^-$, is generated by

$$\boldsymbol{X}_{i,k}^- = \boldsymbol{S}_k^-\boldsymbol{\zeta}_i + \hat{\boldsymbol{x}}_k^-, \quad i = 1, 2, \ldots, 2n \tag{10}$$

where $\boldsymbol{S}_k^-$ is obtained by the Cholesky decomposition of $\boldsymbol{P}_{xx,k}^-$. Then, according to the following relations, the predicted measurements $\hat{\boldsymbol{z}}_k^-$, the measurement error covariance $\boldsymbol{P}_{zz,k}^-$, and the cross-covariance $\boldsymbol{P}_{xz,k}^-$ are computed.

$$\boldsymbol{Z}_{i,k}^- = h(\boldsymbol{X}_{i,k}^-) \tag{11}$$

$$\hat{\boldsymbol{z}}_k^- = \frac{1}{2n}\sum_{i=1}^{2n} \boldsymbol{Z}_{i,k}^- \tag{12}$$

$$\boldsymbol{P}_{zz,k}^- = \frac{1}{2n}\sum_{i=1}^{2n} \left[\boldsymbol{Z}_{i,k}^-(\boldsymbol{Z}_{i,k}^-)^\top - \hat{\boldsymbol{z}}_k^-(\hat{\boldsymbol{z}}_k^-)^\top\right] + \boldsymbol{R}_k \tag{13}$$

$$\boldsymbol{P}_{xz,k}^- = \frac{1}{2n}\sum_{i=1}^{2n} \left[\boldsymbol{X}_{i,k}^-(\boldsymbol{Z}_{i,k}^-)^\top - \hat{\boldsymbol{x}}_k^-(\hat{\boldsymbol{z}}_k^-)^\top\right] \tag{14}$$

A linear batch-mode regression (BMR) model is derived to facilitate matrix-based solutions, improve computational efficiency, and avoid matrix singularity [13]. Following the detailed procedure explained in [4], this yields the following linear regression model:

979-8-3315-8138-1

$$\underbrace{\begin{bmatrix} \boldsymbol{z}_k + \boldsymbol{H}_k \hat{\boldsymbol{x}}_k^- - \hat{\boldsymbol{z}}_k^- \\ \hat{\boldsymbol{x}}_k^- \end{bmatrix}}_{\underline{\boldsymbol{z}}_k} = \underbrace{\begin{bmatrix} \boldsymbol{H}_k \\ \boldsymbol{I}_{n_s} \end{bmatrix}}_{\underline{\boldsymbol{H}}_k} \boldsymbol{x}_k + \underbrace{\begin{bmatrix} \boldsymbol{v}_k \\ \boldsymbol{\epsilon}_k^- \end{bmatrix}}_{\underline{\boldsymbol{e}}_k} \tag{15}$$

Here, $\underline{\boldsymbol{z}}_k$ is the BMR measurement vector, consisting of n_m measurements and n_s predicted states; $\underline{\boldsymbol{e}}_k$ is the BMR error vector that its covariance is defined by (16) [12]; $\boldsymbol{I}_{n_s}$ is the identity matrix; and $\boldsymbol{H}_k$ is the statistical linerization regression matrix, defined as $\boldsymbol{H}_k = \left((\boldsymbol{P}_{xx,k}^-)^{-1}\boldsymbol{P}_{xz,k}^-\right)^\top$.

$$\underline{\boldsymbol{S}}_k = \text{Blkdiag}\left(\boldsymbol{R}_k + \tilde{\boldsymbol{R}}_k,\, \boldsymbol{P}_{xx,k}^-\right) \tag{16}$$

In (16), $\tilde{\boldsymbol{R}}_k$ is defined by (17) to compensate for higher-order Taylor series expansion error terms [12].

$$\tilde{\boldsymbol{R}}_k = \boldsymbol{P}_{zz,k}^- - (\boldsymbol{P}_{xz,k}^-)^\top(\boldsymbol{P}_{xx,k}^-)^{-1}(\boldsymbol{P}_{xz,k}^-) \tag{17}$$

To enhance the resilience and robustness against outliers caused by FDIAs or data loss, this paper employs the PWLS algorithm, which incorporates a penalty term into the objective function of the WLS optimization problem [9], as defined by

$$(\hat{\boldsymbol{x}}_k\ , \hat{\boldsymbol{w}}_k) = \arg\min_{\boldsymbol{x}_k, \boldsymbol{w}_k} \{(\underline{\boldsymbol{z}}_k - \underline{\boldsymbol{H}}_k\boldsymbol{x}_k)^\top \boldsymbol{W}_k\, (\underline{\boldsymbol{z}}_k - \underline{\boldsymbol{H}}_k\boldsymbol{x}_k) \\ + \sum_{i=1}^{n_m+n_s} \lambda \left\|\log(w_{k,i})\right\|_1\} \tag{18}$$

where the vector $\boldsymbol{w}_k$ contains all the diagonal elements of $\boldsymbol{W}_k$, where $w_{k,i}$ denotes the i-th element of $\boldsymbol{W}_k$. The parameter λ is a tuning (forgetting) factor within the range of (0, ∞), which regulates the detection of outliers. The term $\|.\|_1$ represents the norm-1 operator. The penalty term $\lambda \left\|\log(w_{k,i})\right\|_1$ determines the weights for each measurement between 0 and 1 (i.e., $0 \leq w_{k,i} \leq 1$). A weight close to 0 indicates an attacked or suspicious measurement, while a value near 1 reflects a healthy, reliable one. By assigning such weights, PWLS not only detects manipulated or missing measurements but also suppresses their influence in the final state estimation [9].

Algorithm 1 shows the solution of the CKF correction step by incorporating the PWLS technique to solve the bi-convex objective function in (18) [9]. In this algorithm, ϵ is the convergence tolerance, and $\hat{\boldsymbol{w}}_k$ is the weight vector at time step k. The iteration index is j, and $\odot$ denotes the element-wise (Hadamard) product. The i-th measurement residual $r_{k,i}$ is the i-th entry of $\underline{\boldsymbol{z}}_k - \underline{\boldsymbol{H}}_k\boldsymbol{x}_k$. The vectors $\underline{\boldsymbol{z}}_k$ and $\underline{\boldsymbol{H}}_k$ are adjusted via element-wise multiplication with the latest $\boldsymbol{w}_k$, giving $\underline{\boldsymbol{z}}_k^{adj}$ and $\underline{\boldsymbol{H}}_k^{adj}$. Each $\boldsymbol{w}_{k,i}$ is kept in [0, 1]; values outside this range are set to 1, ensuring that larger weights correspond to smaller residuals and higher estimation accuracy [9]. At the end of the algorithm, the covariance matrix of the corrected state errors at time step k, $\boldsymbol{P}_{xx,k}$, is computed [12].

Algorithm 1 PWLS-based CKF Correction Step

Requirements: $\underline{\boldsymbol{S}}_k$, $\underline{\boldsymbol{H}}_k$, and $\underline{\boldsymbol{z}}_k$
Initialize $\boldsymbol{w}_k^{(0)} = [\boldsymbol{0}_{1\times n_m}\ \boldsymbol{1}_{1\times n_s}]^\top$
$\boldsymbol{x}_k^{(0)} = \hat{\boldsymbol{x}}_k^-$
let j = 1
while not converged **do**
  $[update\ \hat{\boldsymbol{x}}_k]$
  $\underline{\boldsymbol{z}}_k^{adj} = \boldsymbol{w}_k^{(j-1)} \odot \underline{\boldsymbol{z}}_k$
  $\underline{\boldsymbol{H}}_k^{adj} = \boldsymbol{w}_k^{(j-1)} \odot \underline{\boldsymbol{H}}_k$
  $\boldsymbol{x}_k^{(j)} = \left(\underline{\boldsymbol{H}}_k^{adj^\top} \underline{\boldsymbol{S}}_k^{-1} \underline{\boldsymbol{H}}_k^{adj}\right)^{-1} \underline{\boldsymbol{H}}_k^{adj^\top} \underline{\boldsymbol{S}}_k^{-1} \underline{\boldsymbol{z}}_k^{adj}$
  $[update\ \hat{\boldsymbol{w}}_k]$
  $\boldsymbol{r}_k^{(j)} = \underline{\boldsymbol{z}}_k - \underline{\boldsymbol{H}}_k\boldsymbol{x}_k^{(j)}$
  If $\lambda/(r_{k,i}^{(j)})^2 < 1$ let $\boldsymbol{w}_{k,i}^{(j)} = \lambda/(r_{k,i}^{(j)})^2$, else $\boldsymbol{w}_{k,i}^{(j)} = 1$
  $j = j + 1$
  If $\left\|\boldsymbol{x}_{k,i}^{(j)} - \boldsymbol{x}_{k,i}^{(j-1)}\right\|_\infty < \epsilon$, then break the loop.
end while
$\boldsymbol{w}_k = \boldsymbol{w}_k^{(j)}$
$\hat{\boldsymbol{x}}_k = \boldsymbol{x}_k^{(j)}$
$\boldsymbol{P}_{xx,k} = \left(\underline{\boldsymbol{H}}_k^\top \boldsymbol{W}_k^{-1} \underline{\boldsymbol{H}}_k\right)^{-1}$

III. Case Studies and Simulation Results

This section evaluates the performance of the proposed PWLS-CKF algorithm for estimating algebraic and dynamic variables under FDIAs and data-loss conditions. The IEEE 39-bus test system was used as the benchmark for the simulations and case studies in this section. Further details are available in [5]. The PMU set $\mathcal{P} = 1,\ 2,\ 6,\ 9,\ 10,\ 13,\ 14,\ 17,\ 19,\ 20,\ 22,\ 23,\ 25,\ 29$ is selected based on the optimal placement strategy in [5] to enhance system observability. In this system, PMUs transmit measurement data in packets at a rate of 100 frames per second. Dynamic behavior is simulated by applying 50% step decreases to the active and reactive power demands at buses 7, 4, 8, and 39 at $t = 0.1$ s, followed by 50% step increases at buses 20, 21, 23, and 24 at $t = 0.5$ s. For all simulation scenarios, the DSE parameters are tuned as follows: $\boldsymbol{R} = 10^{-4}\boldsymbol{I}_{n_m\times n_m}$, $\boldsymbol{Q} = 10^{-10}\boldsymbol{I}_{n_s\times n_s}$, $\boldsymbol{P}_0 = 10^{-8}\boldsymbol{I}_{n_s\times n_s}$, and $\lambda = 10^{-5}$, where $n_s = 98$ and $n_m = 110$ denote the number of state variables and measurements, respectively. Since KF-based DSE methods are designed assuming Gaussian noise and may diverge under non-Gaussian conditions, it is assumed here that, in all scenarios, the measurements are further corrupted by Gaussian noise with a standard deviation of 10^{-3}.

To assess the estimation performance of the proposed approach across various scenarios, the mean absolute error (MAE) metric is employed, defined as

$$\text{MAE} = \frac{1}{n_s n_t}\sum_{k=1}^{n_t} ||\boldsymbol{x}_k^{true} - \hat{\boldsymbol{x}}_k||_1 \tag{19}$$

where $||.||_1$ denotes the Taxicab norm; n_t is the number of samples; and $\boldsymbol{x}_k^{true}$ represents the true state at sample k.

A. Performance Under FDIAs

To illustrate the capability of the proposed PWLS-CKF method in mitigating FDIAs, it is assumed that an at-

979-8-3315-8138-1

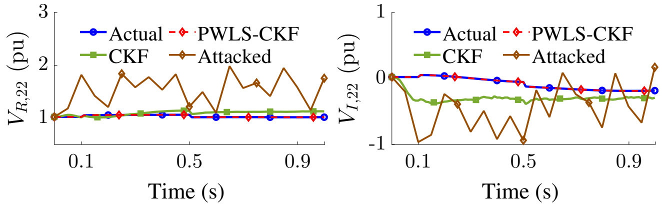

(a) (b)

Fig. 1: Algebraic state variables under the FDIA described in Section III-A: (a) $V_{R,22}$, and (b) $V_{I,22}$.

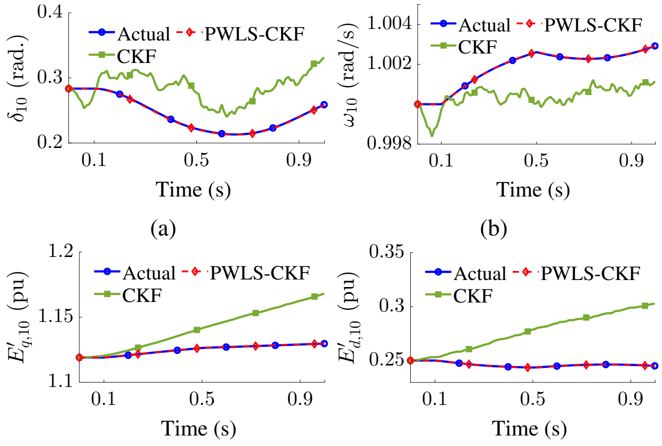

(a) (b) (c) (d)

Fig. 2: Dynamic states of Generator 10 under the FDIA described in Section III-A: (a) δ, (b) ω, (c) E'_q, and (d) E'_d.

tacker randomly compromises measured voltage phasors from PMUs installed at buses 9, 22, 23, and 25. It is assumed that the attacker has full knowledge of the system and can intercept PMU data by accessing routers and injecting false data. Fig. 1 shows the estimated real and imaginary voltages at bus 22 using both CKF and PWLS-CKF methods, with the attacked signals depicted in brown. Fig. 2 presents the corresponding estimates of dynamic variables for generator 10. The results clearly demonstrate that the conventional CKF algorithm fails to track the true system states under an FDIA, resulting in significant estimation errors. In contrast, PWLS-CKF successfully detects and mitigates the attack, maintaining accurate estimations throughout. As confirmed by the MAE values reported in Table I, PWLS-CKF significantly outperforms the CKF algorithm under FDIA conditions.

To further evaluate the accuracy of the PWLS-CKF algorithm, it was tested over 30,090 FDIA scenarios, with some measurements randomly compromised at each step. It detected 98.1% of attacks with no false positives; the 1.9% false negatives were mainly low-magnitude signals. Despite this, the average state MAE remained low (1.71×10^{-4}), showing that attacks on low-magnitude signals have minimal impact and that PWLS-CKF reliably detects mitigates FDIAs while maintaining accurate state estimates.

B. Performance Under Data Loss

To demonstrate the robustness of the proposed method against data loss, it is assumed that measurements from PMUs 1, 2, 9, and 17 fail to reach the control centre due to communication network failure. Fig. 3 depicts the estimated real and imaginary voltages at buse 17 using both CKF and PWLS-CKF methods, while Fig. 4 shows the corresponding dynamic variable estimates for generator 5. The results indicate that the conventional CKF struggles to track the true system states under data loss, leading to notable estimation errors. In contrast, PWLS-CKF effectively detects and mitigates these issues, maintaining accurate estimates. As reflected by the MAE values in Table I, PWLS-CKF substantially outperforms CKF under data loss conditions.

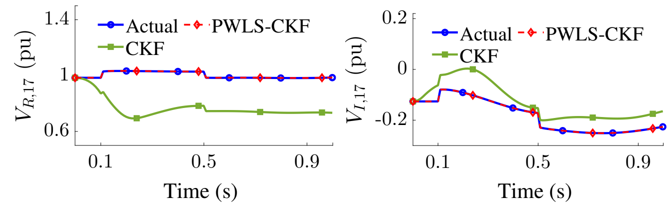

(a) (b)

Fig. 3: Algebraic state variables under the scenario described in Section III-B: (a) $V_{R,17}$, and (b) $V_{I,17}$.

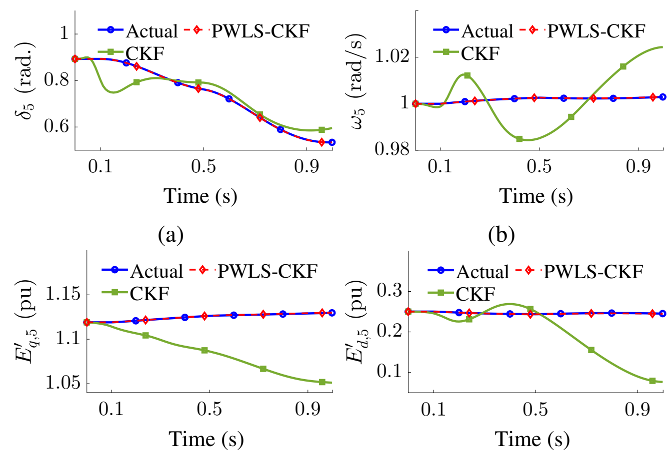

(a) (b) (c) (d)

Fig. 4: Dynamic states of Generator 5 under the scenario described in Section III-B: (a) δ, (b) ω, (c) E'_q, and (d) E'_d.

TABLE I: MAE index for PWLS-CKF and other methods.

	CKF	GM-EKF	GM-UKF	PWLS-CKF
FDIA+Noise	0.0532	0.0017	0.00026	0.00018
Data Loss+Noise	0.1638	0.00096	0.00025	0.00023

To further assess the accuracy of the PWLS-CKF algorithm, it was tested over 30,090 data loss scenarios, in which data from a randomly selected subset of PMUs was dropped at each time step. The algorithm detected 93.9% of missing measurements with no false positives; the remaining 6.1% of undetected cases were primarily low-magnitude signals, similar to the FDIA observations. Despite this, the average state MAE remained low (1.72×10^{-4}), indicating that low-magnitude data loss has minimal impact and that PWLS-CKF effectively detects and mitigates data loss.

C. Comparative Analysis

In this section, the proposed method is evaluated against the GM-UKF–based DSE from [14] and the GM-EKF–based DSE from [11] under the FDIA and data-loss scenarios described in case studies III-A and III-B, respectively. Table I

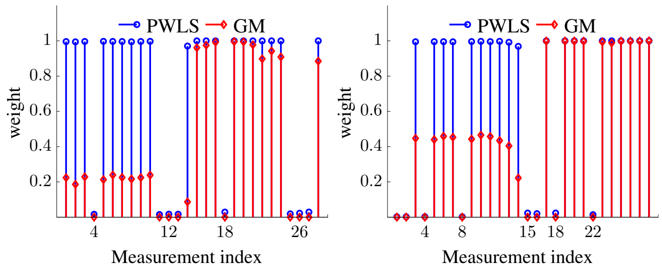

(a) (b)

Fig. 5: Estimated measurement weights from the PWLS and GM methods: (a) under FDIA, and (b) under data loss.

shows that under both FDIA and data-loss conditions, the PWLS-CKF method achieves lower MAE, indicating higher accuracy. The GM-EKF, relying on Jacobian-based linearization, is less effective at mitigating noise, which explains its higher MAE compared to the nonlinear GM-UKF and PWLS-CKF methods.

Fig. 5 shows that the GM method reduces not only the weights of compromised measurements but also of normal ones, whereas PWLS targets only bad measurements. This limitation stems from GM's initial projection statistics (PS) step, which can mistakenly downweight normal voltages when their predictions are inaccurate. Such errors produce larger innovations that violate the Gaussian assumption, causing PS values to deviate from the expected chi-square distribution [14]. Consequently, normal measurements may be underweighted, making it harder for GM to distinguish true outliers and reliably detect attacks, while PWLS maintains accurate detection.

D. Computational Complexity and Real-Time Performance

To evaluate the computational complexity of the proposed PWLS-CKF scheme, the total number of floating-point operations (FLOPs) per iteration is estimated. Let n and m denote the numbers of state variables and measurements, respectively. Under the dense-matrix operation model, the main components have the following costs: prediction $O(n^3)$, batch-mode matrix construction $O(mn^2) + O(m^3) + O(n^3)$, PWLS update $O(mn^2)$, and final CKF update $O(n^3)$. Overall, the total complexity per iteration is approximately $3O(n^3) + O(m^3) + 2O(mn^2)$.

As an example, for the IEEE 39-bus system with $n = 98$ and $m = 110$, the estimated runtime is about 1.57 ms per iteration. This estimate assumes execution on a processor described in [16], operating at 2 GHz and capable of 8 FLOPs per cycle, excludes memory access latency, and assumes the processor is fully dedicated to computation. Since this is well below the 10-ms PMU reporting interval, the proposed scheme is suitable for real-time implementation, enabling continuous dynamic state tracking and robust operation under FDIAs and data loss.

IV. Conclusion

This paper proposes a robust PWLS-CKF–based DSE framework that enables simultaneous estimation of dynamic and algebraic states through an NDAE-based model. By explicitly identifying and down-weighting compromised or missing measurements, the method improves resilience against FDIAs and communication failures. Simulation results on the IEEE 39-bus system confirm that the proposed approach maintains high estimation accuracy and satisfies real-time computational requirements, making it suitable for online monitoring and operation of modern power systems. The proposed framework is particularly relevant for power systems with limited PMU coverage, where reliable estimation of algebraic variables is critical for situational awareness and control.

Future work will investigate the robustness of the proposed method under coordinated FDIAs that aim to remain stealthy by keeping measurement residuals small.

References

[1] J. Zhao and et al., "Roles of dynamic state estimation in power system modeling, monitoring and operation," *IEEE Trans. Power Syst.*, vol. 36, no. 3, pp. 2462–2472, May 2021.

[2] J. Zhao, A. Gómez-Expósito, M. Netto, L. Mili, A. Abur, V. Terzija, I. Kamwa, B. Pal, A. K. Singh, J. Qi, Z. Huang, and A. P. S. Meliopoulos, "Power system dynamic state estimation: Motivations, definitions, methodologies, and future work," *IEEE Trans. on Power Systems*, vol. 34, no. 4, pp. 3188–3198, 2019.

[3] N. Zhou, D. Meng, Z. Huang, and G. Welch, "Dynamic state estimation of a synchronous machine using pmu data: A comparative study," *IEEE Trans. Smart Grid*, vol. 6, no. 1, pp. 450–460, Jan. 2015.

[4] Y. Wang, Z. Yang, Y. Wang, Z. Li, V. Dinavahi, and J. Liang, "Resilient dynamic state estimation for power system using cauchy-kernel-based maximum correntropy cubature kalman filter," *IEEE Trans. Instrum. Meas*, vol. 72, pp. 1–11, 2023.

[5] S. Chakrabarti and E. Kyriakides, "Optimal placement of phasor measurement units for power system observability," *IEEE Trans. Power Syst.*, vol. 23, no. 3, pp. 1433–1440, Aug. 2008.

[6] J. Zhang, G. Welch, G. Bishop, and Z. Huang, "A two-stage kalman filter approach for robust and real-time power system state estimation," *IEEE Trans. Sustain. Energy*, vol. 5, no. 2, pp. 629–636, Apr. 2014.

[7] A. Rouhani and A. Abur, "Linear phasor estimator assisted dynamic state estimation," *IEEE Trans. Smart Grid*, vol. 9, no. 1, pp. 211–219, Jan. 2018.

[8] M. Nadeem, S. A. Nugroho, and A. F. Taha, "Dynamic state estimation of nonlinear differential algebraic equation models of power networks," *IEEE Trans. Power Syst.*, vol. 38, no. 3, pp. 2539–2552, May 2023.

[9] S. Riahinia, A. Ameli, M. Ghafouri, and A. Yassine, "An adaptive penalized weighted least squared approach for detecting and mitigating cyber-attacks on dynamic state estimation," *IEEE Trans. Instrum. Meas.*, 2024.

[10] Z. Kazemi, A. A. Safavi, F. Naseri, L. Urbas, and P. Setoodeh, "A secure hybrid dynamic-state estimation approach for power systems under false data injection attacks," *IEEE Trans. Ind. Inform*, vol. 16, no. 12, pp. 7275–7286, Dec. 2020.

[11] J. Zhao, M. Netto, and L. Mili, "A robust iterated extended kalman filter for power system dynamic state estimation," *IEEE Trans. Power Syst.*, vol. 32, no. 4, pp. 3205–3216, Jul. 2017.

[12] J. Zhao and L. Mili, "A robust generalized-maximum likelihood unscented kalman filter for power system dynamic state estimation," *IEEE J. Sel. Topics Signal Process.*, vol. 12, no. 4, pp. 578–592, Aug. 2018.

[13] Y. Chakhchoukh, H. Lei, and B. K. Johnson, "Diagnosis of outliers and cyber attacks in dynamic pmu-based power state estimation," *IEEE Trans. Power Syst.*, vol. 35, no. 2, pp. 1188–1197, Mar. 2020.

[14] J. Zhao, L. Mili, and A. Gómez-Expósito, "Constrained robust unscented kalman filter for generalized dynamic state estimation," *IEEE Trans. Power Syst.*, vol. 34, no. 5, pp. 3637–3646, Sep. 2019.

[15] P. W. Sauer and M. A. Pai, *Power System Dynamics and Stability*. Champaign, IL: Stipes Publishing, 1998.

[16] *Arm Cortex-A75 Core Technical Reference Manual*, Revision: r3p1 ed., ARM Holdings, San Jose, California, USA, Jul. 2018.

979-8-3315-8138-1